Neoplasia 44 (2023) 100935

Contents lists available at ScienceDirect

Neoplasia

journal homepage: www.elsevier.com/locate/neo

HSP90 C-terminal domain inhibition promotes VDAC1 oligomerization via decreasing K274 mono-ubiquitination in Hepatocellular Carcinoma

Jinxin Zhang [a], Lixia Liu [a], Yan Li [a], Yaling Huang [a], Senbo Xiao [b], Zihao Deng [a], Zhenming Zheng [a], Jieyou Li [a], Manfeng Liang [a], Guantai Xie [a], Xiao Chen [a], Yaotang Deng [a], Wenchong Tan [a], Hairou Su [a], Guibing Wu [a], Chunqing Cai [a], Xuemei Chen [a,1,*], Fei Zou [a,*]

[a] Department of Occupational Health and Occupational Medicine, Guangdong Provincial Key Laboratory of Tropical Disease Research, School of Public Health, Southern Medical University, Guangzhou 510515, China

[b] Nanomechanical Lab (Nanomechanical Lab - NTNU) Department of Structural Engineering Norwegian University of Science and Technology Trondheim, Norway

ARTICLE INFO

Keywords:
Voltage-dependent anion-selective channel protein 1
Heat shock protein 90 inhibitor
Oligomerization
Apoptosis
Hepatocellular carcinoma

ABSTRACT

Voltage-dependent anion-selective channel protein 1 (VDAC1) is the most abundant protein in the mitochondrial outer membrane and plays a crucial role in the control of hepatocellular carcinoma (HCC) progress. Our previous research found that cytosolic molecular chaperone heat shock protein 90 (Hsp90) interacted with VDAC1, but the effect of the C-terminal and N-terminal domains of Hsp90 on the formation of VDAC1 oligomers is unclear. In this study, we focused on the effect of the C-terminal domain of Hsp90 on VDAC1 oligomerization, ubiquitination, and VDAC1 channel activity. We found that Hsp90 C-terminal domain inhibitor Novobiocin promoted VDAC1 oligomerization, release of cytochrome c, and activated mitochondrial apoptosis pathway. Atomic coarse particle modeling simulation revealed C-terminal domain of Hsp90α stabilized VDAC1 monomers. The purified VDAC1 was reconstituted into a planar lipid bilayer, and electrophysiology experiments of patch clamp showed that the Hsp90 C-terminal inhibitor Novobiocin increased VDAC1 channel conductance via promoting VDAC1 oligomerization. The mitochondrial ubiquitination proteomics results showed that VDAC1 K274 mono-ubiquitination was significantly decreased upon Novobiocin treatment. Site-directed mutation of VDAC1 (K274R) weakened Hsp90α-VDAC1 interaction and increased VDAC1 oligomerization. Taken together, our results reveal that Hsp90 C-terminal domain inhibition promotes VDAC1 oligomerization and VDAC1 channel conductance by decreasing VDAC1 K274 mono- ubiquitination, which provides a new perspective for mitochondria-targeted therapy of HCC.

Introduction

Hepatocellular carcinoma (HCC) is the 3rd leading cancer-related death worldwide. As most HCC patients are diagnosed at an advanced stage, precise therapies for HCC and the in-depth mechanism still need to be further explored to decrease mortality [1,2].

Voltage-dependent anion-selective channel protein 1 (VDAC1) is the most abundant protein in the outer-mitochondrial membrane (OMM), the gate between cytosol and mitochondria, thus plays a crucial role in the control of HCC progression and mitochondrial apoptosis pathway [3,4,5]. Mitochondria contain a panel of apoptotic factors, including cytochrome c (Cyto c), AIF, and Smac/Diablo [6,7]. Under physiological conditions, apoptotic factors are typically located in the intermembrane space of mitochondria (IMS). However, upon apoptotic stimulation, VDAC1 oligomerization can form a large channel to export pro-apoptotic proteins like Cyto c from the IMS to the cytoplasm to initiate mitochondrial apoptosis pathway [8,9].

Till now, different strategies targeting VDAC1 show the promising effects in HCC, such as small molecules or peptides directly decreasing VDAC1 level or function, have multiple effects on HCC, leading to mitochondrial dysfunction and impairment of cell energy and metabolism homeostasis, with decreased cell proliferation and cell death [10,11]. Besides directly decreasing VDAC1 level, targeting VDAC1 oligomerization has been another hot spot for various diseases, such as using VDAC1 oligomerization inhibitor VBIT4 to decrease apoptosis to prevent neuron damage in Alzheimer's Disease (AD) [12]. Different from

* Correspondence authors.
E-mail addresses: cxmcsz@smu.edu.cn (X. Chen), zfei@smu.edu.cn (F. Zou).
[1] Lead Contact.

https://doi.org/10.1016/j.neo.2023.100935
Received 14 July 2023; Received in revised form 21 August 2023; Accepted 5 September 2023

neuron protective purpose for AD, many cancer therapies aim to induce VDAC1 oligomerization and apoptosis [13], but the detailed mechanism still needs to be elucidated to explore precise targets.

We found that cytosolic Hsp90α bound to dozens of mitochondria-related proteins, and the most abundant one was VDAC1(See unpublished Fig 1). Heat shock protein 90 (Hsp90) is a family of ubiquitous and highly conserved molecular chaperones, comprises ~1–2 % of total protein content and Hsp90 expression is elevated to ~4–6 % of all cellular proteins in cancer cells. Hsp90 has ~400 partner proteins, most of which are highly associated with cancer-related signaling pathways. The partner proteins rely on hsp90 for their activation, stabilization and maturation [14–17]. Hsp90 forms a homodimer with each monomer consisting of three domains, an ATP-binding N-terminal domain (NTD) with ATPase activity, a middle domain (MD), and a C-terminal domain (CTD) that is responsible for dimerization and cochaperone binding [16,17]. In cancer cells, Hsp90 levels are upregulated due to the excessive need to fold overexpressed and mutated proteins, and many of the 400 partner proteins are associated with the ten hallmarks of cancer. This makes Hsp90 especially vital in the initiation, progression and/or metastasis of cancer cells. Therefore, inhibition of Hsp90 has been pursued as a combination therapy to selectively target cancer cells and simultaneously disable multiple oncogenic signaling pathways [17].

In HCC, Hsp90 is upregulated in clinical samples and is associated with poor clinical outcomes [18,19]. More evidence has shown that Hsp90 plays an important role in HCC progression and prognosis [20–23]. Although the Hsp90 protein folding machinery has been extensively studied, the exact mechanism is not fully understood. Up to date, there have been 134 Hsp90-related clinical evaluations for different cancer types, and 16 trials are still active (clinicaltrials.gov). Nineteen Hsp90 N-terminal inhibitors have entered clinical trials, but most have failed to gain FDA approval due to toxicities resulting from pan-inhibitory activity and their ability to induce the heat shock response (HSR) [24]. Under cellular stress, HSR leads to upregulation of Hsp90 and other heat shock proteins to promote cell survival, which requires a higher concentration of inhibitors to inhibit Hsp90 levels, increasing the toxic side effects of Hsp90 inhibitors such as hepatotoxicity and visual impairment. In particular, it has been found that although Hsp90 N-terminal inhibitors inhibit tumor growth, they may promote tumor metastasis [25,26]. Therefore, C-terminal inhibition offers a valuable alternative to target cancer cells without induction of the HSR [17,27].

Novobiocin was first found as Hsp90 inhibitor, which was found to bind to Hsp90 C-terminal (amino acid 657-677, ATP binding site) by Nerckes [17,27,28]. Though various new analogs are developed afterward, the detailed inhibition mechanism of Novobiocin still needs to be further explored for the development of Hsp90 C-terminal inhibitors.

In this study, we focused on the effect of the Hsp90 C-terminal domain inhibitor Novobiocin on VDAC1 oligomerization, ubiquitination, and VDAC1 channel activity, which may provide a new application of Hsp90 inhibitors for mitochondria-targeted therapy of HCC.

Materials and Methods

Reagents and cells

HepG2 (SCSP-510) cell line was purchased from the Cell Bank of the Chinese Academy of Medical Sciences. HepG2-Luc cell line was purchased from Cloud-Clone Corp. (Wuhan, China). All cell lines were authenticated, and cells were thawed upon arrival, expanded, and stored in a liquid nitrogen tank. The absence of mycoplasma cell contamination was confirmed by MycAwayTM-Color One-Step Mycoplasma Detection Kit (40611ES, Yeasen, Shanghai, China). All the cell lines were cultured in Dulbecco's Modified Eagle's Medium (DMEM, Gibco, MA, USA) with 10 % fetal bovine serum (Gibco, MA, USA) at 37°C, and 5% CO_2 atmosphere. Ganetespib (STA9090; S1159), Novobiocin (NB; S2492), VBIT-4 (HY-129122), and MG132 (S2619) were purchased from SelleckChem (Houston, TX, USA).

Plasmids

The HA-tag fusion of Hsp90α full-length, the N-terminal nucleotide-binding domain (NTD), the middle domain (MD), and the C-terminal dimerization domain (CTD) of Hsp90α were kind gifts from Matthias Mayer (ZMBH, Heidelberg University, Heidelberg, Germany). VDAC1 WT plasmid was cloned into pcDNA3.1 neo (+) N-terminal HA-tagged vector. VDAC1 K274 mutant (K274R) was generated by site-directed point mutagenesis (Hanheng Biotechnology Co., Ltd., Shanghai, China) [29].

Cell proliferation assay

Cell colony assay was performed with crystal violet. Cells were seeded in 6-well plates (1×10^5 cells/well) and were cultured for 72 h with normal medium. Cells were fixed and stained with 0.5% crystal violet solution in 20% methanol. Images of the wells were taken with a wide-field microscope (Olympus, Tokyo, Japan), and the number of colonies was counted [30].

Label-free quantitative proteomic of mitochondrial ubiquitination analysis

After mitochondria were extracted [31], the samples in lysis buffer (8 M urea, 1% Protease Inhibitor Cocktail) were sonicated three times on ice with a high intensity ultrasonic processor. The remaining debris was removed by centrifugation at 12,000 g at 4°C for 10 min. The supernatant was collected, and the protein concentration was determined with BCA kit according to the manufacturer's instructions. After trypsin digestion, the tryptic peptide dissolved in NETN buffer (100 mM NaCl, 1 mM EDTA, 50 mM Tris-HCl, 0.5% NP-40, pH 8.0) were incubated with pre-washed antibody beads (PTM1104, PTM Bio, Jingjie Biotechnology Co., Hangzhou, China) at 4°C overnight with gentle shaking. Then the beads were washed four times with NETN buffer and twice with H_2O. The bound peptides were eluted from the beads with 0.1% trifluoroacetic acid. Finally, the eluted fractions were combined and vacuum-dried. For LC-MS/MS analysis, the resulting peptides were desalted with C18 Zip-Tips (Millipore, Darmstadt, Germany). The tryptic peptides were analyzed by LC-MS/MS on an EASY-nLC 1000 UPLC system. The peptides were subjected to NSI source followed by tandem mass spectrometry (MS/MS) in Q ExactiveTM Plus (Thermo, MA, USA) coupled online to the UPLC. The resulting MS/MS data were processed using Maxquant search engine (v.1.6.6.0). Tandem mass spectra were searched against human Uniprot database concatenated with reverse decoy database.

Western blotting

Western blot analysis was performed as described previously [30]. The following primary antibodies were used: VDAC1 antibodies for VDAC1 oligomerization (1:1000, ab154856, Abcam, Cambridge, UK), VDAC1 antibodies for VDAC1 monoubiquitination (1:1000, sc39099, Santa Cruz, CA, USA), Hsp90α (1:1000, 8165S, Cell Signaling Technology, MA, USA), β-actin (1:6000, RM2001, Ray Antibody Biotech, Beijing, China), HA (1:1000, H3663, Sigma, MO, USA), cytochrome c (1:1000, sc13156, Santa Cruz, CA, USA), COX IV (1:1000, 4844S, Cell Signaling Technology, MA, USA), Tubulin (1:1000, 2128S, Cell Signaling Technology, MA, USA), Ubiquitin (1:1000, 3933s, Cell Signaling Technology, MA, USA), caspase 3 (1:1000, 9662S, Cell Signaling Technology, MA, USA), and PARP (1:1000, 9532S, Cell Signaling Technology, MA, USA) The secondary antibodies (Donkey anti-Mouse/Rabbit/Rat IRDye 680/800) were purchased from Li-COR Biosciences (Lincoln, NE, USA). For the analysis of VDAC1 monoubiquitination, mitochondrial proteins were extracted as described previously (31) and WB analysis was performed. PVDF membranes were

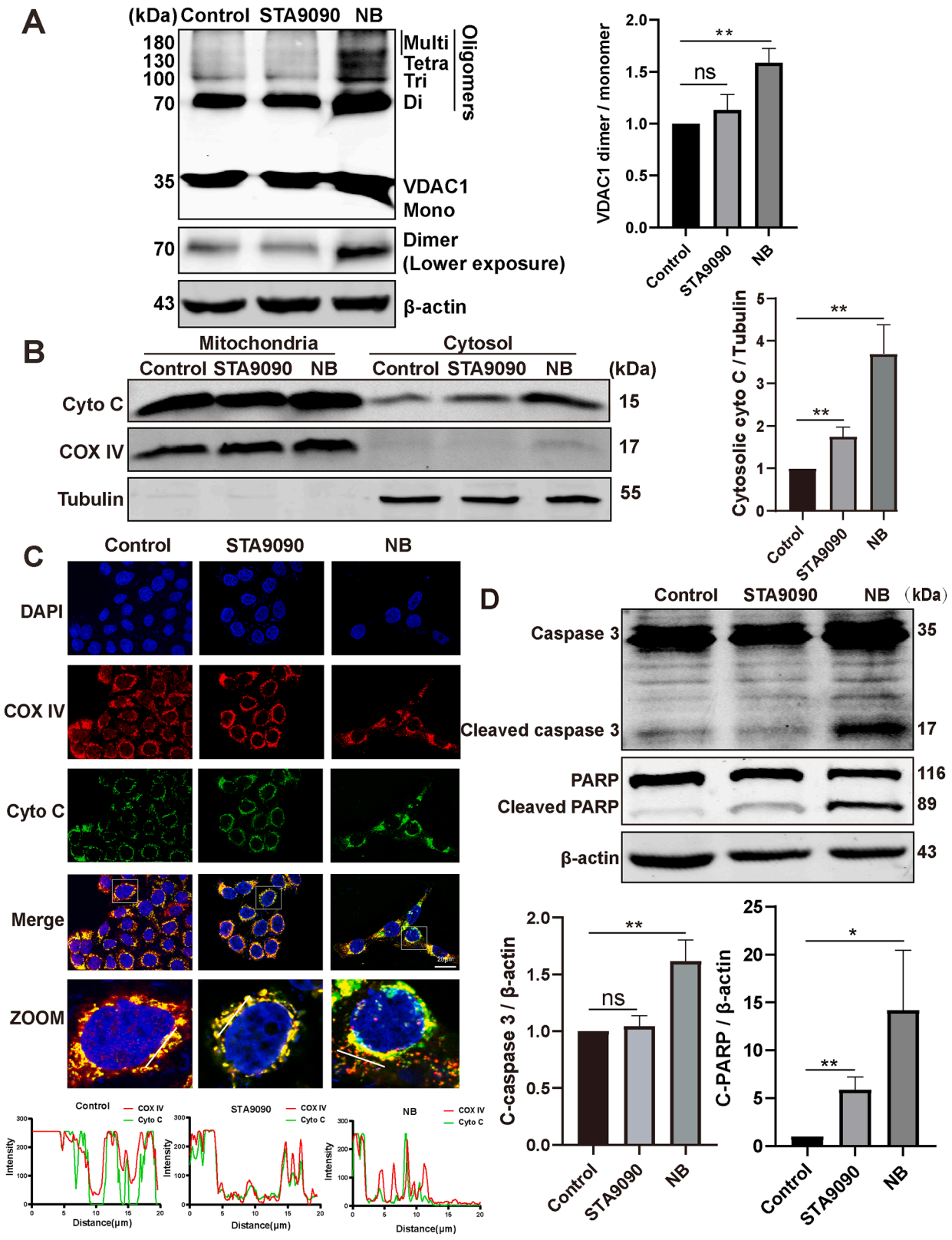

Fig. 1. Hsp90α C-terminal inhibitor Novobiocin (NB) increases VDAC1 oligomerization, cytochrome c release and initiates apoptosis in HepG2 cells. HepG2 cells were set as control, STA9090-treated (100 nM, 24 h) or NB-treated (0.5 mM, 24 h) group. **(A)** After adding the crosslinking reagent ethylene glycolbis (EGS, 500 μM), oligomerization of VDAC1 was visualized by Western blotting. **(B)** Western blotting was performed to determine the level of cytochrome c in the mitochondria and cytosol of HepG2 cells. **(C)** Confocal immunofluorescence images of COXIV (red) and cytochrome c (green) in HepG2 cells. Scale is 20μm. The lower panel was the colocalization analysis of COX IV (red) / Cyto c (green). Scale bar is 20μm. **(D)** Cleavage of Caspase 3 and PARP was detected by Western blotting. All data represent mean ± SD, n = 3, *$p < 0.05$, **$p < 0.01$.

incubated with VDAC1 antibodies (sc13156, Santa Cruz, CA, USA). Blots were scanned with Li-COR Odyssey (Li-COR Biosciences, Lincoln, NE, USA). The band intensities were analyzed by ImageJ software v1.8.0 (NIH, MD, USA).

Immunofluorescence staining and confocal microscopy

Cells were fixed in 4% paraformaldehyde, washed with PBS, and permeabilized with - 20°C precooled methanol. The immunodetection was performed by incubating the cells with mouse anti-cytochrome c (1:200, sc13156, Santa Cruz, CA, USA) and rabbit anti-COX IV (1:200, 4844S, Cell Signaling Technology, MA, USA) at 4°C overnight and subsequently with Alexa Fluor 488 anti-mouse (1:100; A-11001, Life Technologies, CA, USA) and Alexa Fluor 555 anti-Rabbit (1:100; A31572, Life Technologies, CA, USA) antibodies at room temperature for 2 h. Cell nuclei were stained with DAPI for 5 min. Images were obtained by Olympus FV1000 Confocal Laser Scanning Microscope (OLYMPUS, Tokyo, Japan). Colocalization images were analyzed by Image software v1.8.0 (NIH, MD, USA). The analyses were performed in several regions in each image to prevent any bias by imaging or staining artifacts.

VDAC1 cross-linking assay

After harvest, cells were resuspended in PBS (pH 8.0) at 2.5×10^7 cells/ml and then incubated for 15 min at 30°C with the cross-linking reagent, ethylene glycolbis (EGS, 500 μM). To quench additional cross-linker, 1 M Tris (pH 7.5) was introduced (10 mM final conc.) and incubated for 15 min at room temperature. Samples were subjected to SDS-PAGE and immunoblotting using an anti-VDAC1 antibody (ab154856, Abcam, Cambridge, UK) [32].

For VDAC1 cross-linking analysis of xenograft tumors, Cut the tumor into fragments in D-Hank's buffer at 4 ℃, twice-washed through PBS. Add 0.1875% pancreatic enzyme (0.25% pancreatic enzyme: PBS 3:1) to the tumor of each nude mouse, place it in a 37 ℃ incubator for digestion. After 20 minutes, add 0.1% DNA enzyme and then the pellet was filtered through a 70 μm cell strainer. Cells were collected by centrifugation (5 min, 1200 rpm, RT). After harvest, cells were resuspended in PBS (pH 8.0) at 2.5×10^7 cells/ml and then incubated for 15 min at 30°C with the cross-linking reagent, ethylene glycolbis (EGS, 500 μM). To quench additional cross-linker, 1 M Tris (pH 7.5) was introduced (10 mM final conc.) and incubated for 15 min at room temperature. Samples were subjected to SDS-PAGE and immunoblotting using an antiVDAC1 antibody (ab154856, Abcam, Cambridge, UK).

Ultrastructural analysis by transmission electron microscopy (TEM)

After treated with NB or NB combined with VBIT-4, HepG2 cells were fixed in 2.5% glutaraldehyde in PBS buffer pH 7.4 for 1 h at room temperature, postfixed in 2% aqueous osmium tetroxide, dehydrated in gradual ethanol (30–100%) and propylene oxide, embedded in pure epoxy resin for 8 h at 72 °C. Ultra-thin sections were cut and stained with uranyl acetate-lead citrate. After mounted on a 200-mesh copper grid, the ultrastructure of mitochondrial morphology was observed by transmission electron microscopy (Hitachi-7500, Hitachi, Tokyo, Japan) at 60 kV.

Transwell invasion assay

HepG2 cells were treated with NB or NB combined with VBIT-4 for 24 h. The transwell assay was performed in 24-well transwell chambers (Cell Culture Insert: PET Membrane 8 μm, pore size 6.5 mm diameter, #3422, Corning, NY, USA). HepG2 cells were starved and 5×10^4 cells resuspended in 200 μL of basic medium were seeded in the upper chamber coating with Matrigel (1:5 dilution, #356,234, BioCoat, NY, USA). The lower chamber was filled with 600 μl 10% FBS DMEM. After 24 hours, cells in the upper chamber were discarded. The remaining cells were fixed in 4% paraformaldehyde for 20 min and stained with 0.1% crystal violet for 10 min. Take 6 pictures randomly using an Inverted digital imaging microscope (Eclipse TS100LED-F MV, Nikon, Tokyo, Japan) in 10 × objective lens. Invasive cells were counted by ImageJ software v1.8.0 (NIH, MD, USA).

Coarse-grained model simulation

Considering the large molecular structures of the two proteins and the required bilayer lipid membranes in the simulation system, MARTINI coarse-grained force field (version 2.2) was chosen [33]. All the simulations were performed using the Gromacs package (version 2020.6, www.gromacs.org). Both molecular structures were obtained from the RCSB Protein Data Bank, with the PDB id 2CG9 for Hsp90 and 2JK4 for VDAC1, respectively [34,35]. Before converting the all-atom molecular structures to coarse-grained models, the full Hsp90 structure was energy minimized and equilibrated for 20 ns using the all-atom OPLS force field for elimination of any high-energy close contacts. A membrane with VDAC1 molecules was prepared to probe the binding event of Hsp90. Specifically, four coarse-grained VDAC1 molecules were embedded into a periodic dipalmitoylphosphatidylcholine (DPPC) membrane with a surface area of 16×16 nm^2, using the insane toolkit [36]. During the equilibration simulation, VDAC1 could freely float in the membrane, forming different oligomer structures, which were used to build larger simulation systems containing Hsp90 for binding simulations. Finally, the membrane with VDAC1 molecules was combined with Hsp90 molecules in a solution in a large periodic simulation box for longer simulations.

Co-immunoprecipitation

Protein samples extracted from HepG2 cells were incubated with indicated antibody for 4 h at 4°C. Protein A/G-Sepharose beads (Millipore, MA, USA) were added, incubated for 2 h at 4°C, and separated from non-bound material by centrifugation (1000 g, 2 min). Immune complexes were boiled and separated by electrophoresis on 10% SDS-PAGE, and proteins were detected by immunoblotting. Band intensities were analyzed using ImageJ software v1.8.0 (NIH, MD, USA). The following antibodies were used: Hsp90α (8165S, Cell Signaling Technology, MA, USA), VDAC1 (ab154856, Abcam, Cambridge, UK), and HA (H3663, Sigma, MO, USA).

Subcutaneous tumor xenograft in nude mice

All animal experiments were conducted according to Southern Medical University Animal Welfare, and the research protocols were approved by the Institutional Animal Care and Use Committee of Southern Medical University (Approved code L202029). Four-week-old male nude mice (BALB/c) were housed in four mice per cage in a specific pathogen-free room with a 12 h light/dark schedule at 25°C ± 1°C and were fed an autoclaved chow diet and water ad libitum. After a week, the weight of male BALB/c nude mice reached about 18 g and the tumor cells was injected. HepG2-Luc cells (1×10^7 in 200 μl serum-free media) were subcutaneously inoculated on the left/right dorsal side of 5-week-old male BALB/c nude mice. Each experimental group consisted of six animals. At 14 days after injection, tumor-bearing mice were randomly divided into three groups by the tumor volume and the treatment started. STA9090 (dissolved in 10% DMSO, 18% Cremophor RH, 3.6% dextrose, 68.4% ddH_2O at 60°C, 25 mg/kg) or Novobiocin (dissolved in DMSO, 50 mg/kg) was injected intraperitoneally into the mice of STA9090 group or mice of Novobiocin group three times per week for 14 days. The final solution without STA9090 or NB was injected intraperitoneally into mice in the control groups. Xenograft tumor weight and volume was recorded every two days and the volume was calculated as V=0.5 × L × W2 (V: volume, L: length, W: width). After tumor retrieval,

each tumor was cut into 3 parts, one part was frozen and used later for WB; the other part was used for VDAC1 cross-linking assay; the last part was were fixed in 4% paraformaldehyde and used later for immunohistochemistry staining. For VDAC1 cross-linking assay, the tumor of each nude mouse was cut into fragments in D-Hank's buffer at 4 ℃, twice-washed through PBS. Add 0.1875% pancreatic enzyme (0.25% pancreatic enzyme: PBS = 3:1) to the tumor, place it in a 37 ℃ incubator for digestion. After 20 minutes, add 0.1% DNA enzyme and then the pellet was filtered through a 70 μm cell strainer. Cells were collected by centrifugation (5 min,1200 rpm, RT). After harvest, cells were cross-linked by EGS.

Immunohistochemistry (IHC) staining

Xenografts harvested from six mice in each group and one third of each tumor from the indicated groups was fixed in 4% paraformaldehyde for 72 h and processed using the conventional paraffin embedding method. IHC was performed on paraffin sections of xenograft nude mice according to the standard LSAB protocol (BOSTER, Wuhan, China). Primary antibodies were used as follows: cleavage-caspase 3 (1:100, 9661S, Cell Signaling Technology, MA, USA) and cleavage-PARP (1:100, 5625S, Cell Signaling Technology, MA, USA), and isotype-matched IgG was used as a negative control. For quantitative analyses, we used ImageJ software v1.8.0 (NIH, MD, USA) to quantify as average optical density (AOD) [AOD = Integrated Optical Density (IOD) SUM/Area SUM].

VDAC1 purification, channel reconstitution, current recording and analysis

VDAC1 protein was purified from rat liver mitochondria using an elite: hydroxyapatite column as previously described [37]. The purified VDAC1 was reconstituted into a planar lipid bilayer (PLB). Subsequently, whole-cell patch clamp current recordings and data analyses were performed as previously described [38]. Briefly, PLB was prepared from soybean asolectin dissolved in n-decane (30 mg/ml). Purified VDAC1 (~1–2 ng) in the detergent (3% Triton X-100, 10mM Tris-HCl, pH 7.4) was added to the chamber, which was defined as the cis side containing 1 M KCl and 10 mM HEPES, pH 7.4. Currents were recorded before and after the addition of purified Hsp90α (SPR-101C, StressMarq Biosciences, BC, Canada, VDAC1:Hsp90α = 3:1) in the cis compartment, under voltage-clamp using a HEKA EPC10 amplifier (HEKA Electronics, Lambrecht, Germany). The currents measured with respect to the trans side of the membrane (ground), were low-pass-filtered at 1 kHz and digitized online using the HEKA Patchmaster software (HEKA Electronics, Lambrecht, Germany). The offline data visualization and selection were carried out by pCLAMP 10.7(Molecular Devices, San Jose, CA, USA). A significantly long duration (~30 s) of current traces was selected for further data analyses by Origin 2018 software (OriginLab Corp., Northampton, MA, USA). The results were obtained at least in triplicate and the mean and standard error were calculated. Finally, the channel current and conductance of VDAC1 were comparatively analyzed using a Student' s t-test at a 95% confidence level.

Statistical Analysis

All data were presented as the mean ± standard deviation (SD) from three independent experiments. Statistical analyses were performed using SPSS 21.0 software (SPSS, IBM, IL, USA). Comparative analyses were performed using a two-tailed Student's t-test. Multi-parameter analyses were performed using one-way analysis of variance (ANOVA) with subsequent recommended post hoc analyses. Statistical significance was set at $p < 0.05$.

Results

Hsp90 C-terminal inhibitor Novobiocin (NB) increases VDAC1 oligomerization, cytochrome c release and initiates mitochondrial apoptosis pathway

Comparing to Hsp90 N-terminal inhibitor STA9090, Hsp90 C-terminal inhibitor NB triggered significant apoptosis (Fig. S1). Since VDAC1 oligomerization initiates mitochondrial apoptosis pathway through the release of cytochrome c and our Hsp90α interactome results suggested that Hsp90α interacted with dozens of mitochondrial proteins, among which VDAC1 was the most abundant one (See unpublished Fig 1), we wondered whether Hsp90 C-terminal inhibitor Novobiocin induced mitochondria-dependent apoptosis in HepG2 cells through VDAC1 oligomerization. The results showed that Hsp90 C-terminal inhibitor Novobiocin induced significant VDAC1 oligomerization (Fig. 1A) and obvious release of cytochrome c from mitochondria (Fig. 1B), comparing to Hsp90 N-terminal inhibitor STA9090. In addition, we used antibodies of cytochrome c and mitochondrial marker protein COX IV to perform immunofluorescence staining. The confocal microscopy images further supported that Hsp90 C-terminal inhibitor NB increased out-mitochondria-localization of cytochrome c (Fig. 1C), which consistently indicated that NB promoted the release of cytochrome c from mitochondria. Next, we analyzed the cleavage of mitochondrial apoptosis-related proteins induced by cyto c release. The data showed that Hsp90 C-terminal inhibitor NB significantly increased the cleavage of caspase 3 and PARP (Fig. 1D). In conclusion, Hsp90 C-terminal inhibitor NB increases VDAC1 oligomerization, cytochrome c release, and initiates mitochondrial apoptosis pathway.

VDAC1-specific oligomerization inhibitor VBIT-4 alleviates Hsp90 C-terminal inhibitor NB-induced VDAC1 oligomerization and cytochrome c release

To further confirm VDAC1 oligomerization is the key step for apoptosis induced by Hsp90 C-terminal inhibitor NB, we treated HepG2 cells with a VDAC1-specific oligomerization inhibitor (VBIT-4) [39] to observe whether it could alleviate NB-induced VDAC1 oligomerization and apoptosis. EGS chemical crosslinking results showed that VBIT-4 significantly inhibited NB-induced VDAC1 oligomerization (Fig. 2A). Consistent with this result, the release of cytochrome c from mitochondria to cytoplasm was reduced (Fig. 2B), and cleaved caspase 3 and PARP were also decreased (Fig. 2C). Transmission electron microscopy revealed that mitochondrial ultrastructure was severely damaged after NB treatment in HepG2 cells. Mitochondria were swollen, and mitochondrial cristae disappeared or became vacuolated. However, VBIT-4 could restore NB-induced mitochondrial ultrastructure damage, especially in the restoration of mitochondrial cristae disappeared (Fig. 2D). In addition, NB inhibited the proliferation and invasion of HepG2 cells, but VBIT-4 combined with NB treatment restored the proliferative (Fig. 2E) and invasion ability (Fig. 2F) of HepG2 cells. In summary, Hsp90 C-terminal inhibitor NB-induced cytochrome c release and apoptosis are VDAC1 oligomerization dependent. Moreover, induced VDAC1 oligomerization related apoptosis inhibits cell proliferation and invasion, which could be restored by VDAC1 oligomerization inhibitor.

Dysfunction of Hsp90α C-terminal promotes VDAC1 oligomerization

To investigate the regulation of VDAC1 oligomerization by Hsp90, we used atomic coarse particle model [34,35] to simulate the recognition and binding events between Hsp90α and VDAC1. Different states of the VDAC1 molecules in the DPPC membrane were observed at equilibrium. The N-terminal domain of VDAC1 is located in the pore, and Hsp90α binds to VDAC1 on the side away from the C-terminal domain of VDAC1 (Fig. 3A, Fig. S2A). Previous results showed that the C-terminal domain of VDAC1 faces the mitochondrial inter-membrane space [40].

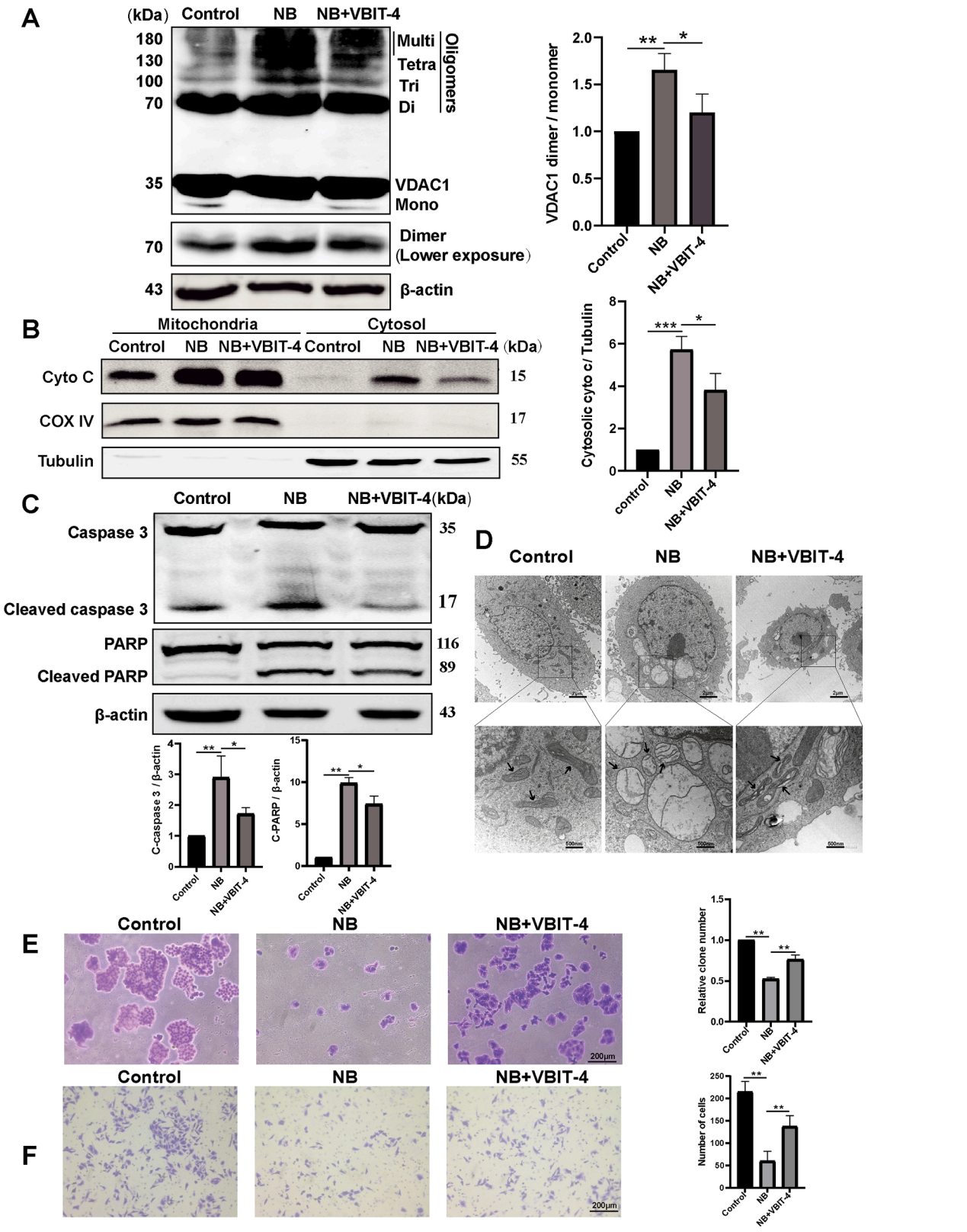

Fig. 2. VBIT-4 ameliorates Novobiocin-induced and VDAC1 oligomerization-related apoptosis in HepG2 cells. **(A)** HepG2 cells were treated with NB (0.5 mM), or NB combined with VBIT-4 (10 μM) for 24 h. The level of VDAC1 dimer was determined by western blot analysis after cross-linking with EGS. **(B)** Western blotting was performed to determine the level of cytochrome c in the mitochondria and cytosol of HepG2 cells. **(C)** The cleavage of caspase3 and PARP were detected by western blotting. All data represent mean ± SD, n = 3, *$p < 0.05$, **$p < 0.01$. **(D)** Transmission electron microscopy discloses the morphology of mitochondria (black arrows) in HepG2 cells on NB (0.5 mM), or NB combined with VBIT-4 (10 μM) treatment. Scale is 2 μm (top panel) or 500 nm (bottom panel). **(E)** Cell proliferation was detected by colony growth assays with crystal violet staining. Representative photographs and bar graphs are from three independent experiments. **(F)** Transwell invasion assays were performed with HepG2 cells treated with NB (0.5 mM), or NB combined with VBIT-4 (10 μM). Scale bar is 200μm. The data are presented as mean ± SD, n=6. *$p < 0.05$, **$p < 0.01$.

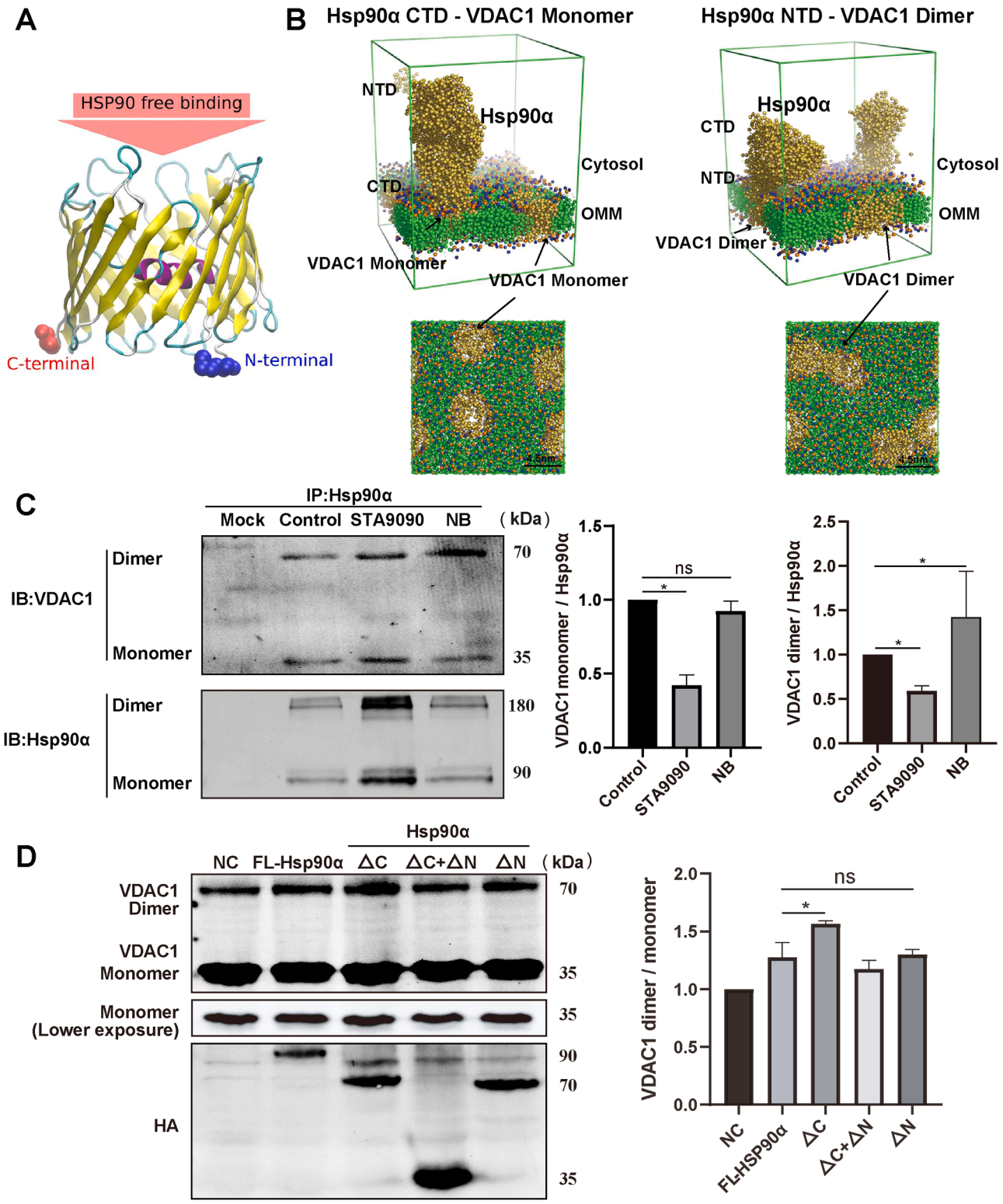

Fig.3. Dysfunction of Hsp90α C-terminal promotes VDAC1 oligomerization. **(A)** Schematic of HSP90 binding direction towards VDAC1 during free binding. **(B)** Atomic coarse particle modeling was used to simulate the interaction of Hsp90α-VDAC1. Typical system snapshot of stable binding complex of Hsp90α with VDAC1 monomer and dimer in the membrane (top panel). Top view of VDAC1 monomer and dimer in the membrane (bottom panel). **(C)** HepG2 cells were incubated with STA9090 (100 nM) or NB (0.5 mM) for 24 h. Co-immunoprecipitation of VDAC1 with Hsp90α was performed with lysates after incubation with cross-linking reagent Ethylene glycolbis (EGS). Hsp90α, VDAC1 monomer and dimer levels were analyzed by immunoblotting. **(D)** HepG2 cells were transiently transfected with plasmids encoding HA-tagged Hsp90α full-length or the HA-tagged NTD-MD (ΔC), MD (ΔC + ΔN), and MD-CTD (ΔN) domains. Cells were then treated with cross-linking reagent EGS. HA and VDAC1 dimer levels were determined by Western blot analysis. All data represent mean ± SD, n = 3,$^{*}p < 0.05, ^{**}p < 0.01$.

Therefore, Hsp90α interacts with VDAC1 on the cytoplasmic side in the coarse particle mode assay. Hsp90α was found to bind to VDAC1 monomer and oligomers (Fig. 3B, Fig. S2A). In different simulation systems with either VDAC1 monomer or dimer, Hsp90α was first allowed to freely diffuse in the system to find and bind with VDAC1 for 10μs. With the large molecular size and the initially relatively small distance to the membrane, Hsp90α was able to interact with VDAC1 molecules in 1 - 2 μs simulation time. Once the interactions occurred, Hsp90α slowly migrated to membrane, showing an obvious decrease pattern in interaction potential. (Fig. S2B). In the last stage of binding, Hsp90α was stably anchored to the VDAC1 molecules, resulting in a stable and low plateau of the interaction potential. The same process of binding was observed during the binding of Hsp90α to both VDAC1 monomer and dimer (Fig. S2C). The C-terminal domain of Hsp90α was found actively participate in binding with cytosolic side of VDAC1, especially in binding with VDAC1 monomers (Fig. 3B, left panel). However, the N-terminal domain of Hsp90α participated at the binding interface with VDAC1 dimer (Fig. 3B, right panel). To further verify the results of coarse-grained molecular systems, we examined the binding of Hsp90α to VDAC1 oligomers by using EGS cross-linking after the treatment of Hsp90 N-terminal inhibitor STA9090 or C-terminal inhibitor NB. The results of the VDAC1 cross-linking combined with co-immunoprecipitation showed that Hsp90 C-terminal inhibitor NB promoted Hsp90α binding to VDAC1 dimer (Fig. 3C), further indicating the dysfunction of Hsp90α C-terminal induced Hsp90-VDAC1 dimer complex formation. To rule out non-specific effects of Hsp90 inhibitors, we transfected the plasmids encoding Hsp90α full-length (FL), NTD, MD, and CTD constructed as HA fusions into HepG2 cells. Our results showed that deletion of C-terminal domain of Hsp90α promoted VDAC1 oligomerization (Fig. 3D). All the above indicates dysfunction of Hsp90α C-terminal promotes VDAC1 oligomer formation via Hsp90-VDAC1 dimer complex formation.

Hsp90α C-terminal inhibition decreases VDAC1 K274 mono-ubiquitination to promote VDAC1 oligomerization and initiate mitochondrial apoptosis pathway

VDAC1 is a key molecule in the process of apoptosis and increased VDAC1 mono-ubiquitination inhibits apoptosis [29]. Since the above data indicated dysfunction of Hsp90α C-terminal promoted VDAC1 oligomerization to initiate mitochondrial apoptosis pathway, we wondered whether Hsp90α regulates VDAC1 oligomerization-related apoptosis by affecting VDAC1 ubiquitination. To prove this, we treated HepG2 cells with Hsp90 N-terminal inhibitor STA9090 or Hsp90 C-terminal inhibitor NB and extracted mitochondria from HepG2 cells for ubiquitination quantitative proteomic analysis [31]. The results showed that mono-ubiquitination of VDAC1 K274 was significantly reduced after NB treatment compared with STA9090 treatment or control group (Fig. 4A, right panel). It has been reported that VDAC1 K274 is the mono-ubiquitination site of VDAC1 and inhibition of VDAC1 K274 mono-ubiquitination promotes apoptosis by enhancing the mitochondrial calcium uptake through mitochondrial calcium uniporter (MCU) [29]. As reported in the literature, MCU interacts with VDAC1 and mediates VDAC1 overexpression-induced cell death in CGNs [41]. And we all know VDAC1 overexpression induces VDAC1 oligomerization [6]. In addition, VDAC1 K274 site is located on β-19 strand of VDAC1 barrel structure, which is consistent with the β-strand where VDAC1 dimer formation site is located [29]. Therefore, we speculated that inhibiting mono-ubiquitination of VDAC1 K274 would promote the formation of VDAC1 oligomers. Then, wild type VDAC1 plasmid (VDAC1 WT) and VDAC1 K274 mutant plasmid (VDAC1 K274R) plasmid, which lost the ability of K272 ubiquitination, were constructed and transfected into HepG2 cells. Notably, HepG2 cells transfected with VDAC1 K274R mutant plasmid exhibited an increase of VDAC1 oligomerization, comparing to the cells transfected with VDAC1 WT plasmid (Fig. 4B). Moreover, more cytochrome c was released from the mitochondria after VDAC1 K274R overexpression (Fig. 4C), and more cleaved Caspase 3 and PARP were observed (Fig. 4D). Taken together, inhibition of VDAC1 K274 mono-ubiquitination promotes VDAC1 oligomerization and initiates mitochondrial apoptosis pathway. Since Parkin regulates the ubiquitination of VDAC1, we examined the translocation of Parkin to mitochondria after treatment with two different Hsp90 inhibitors. The results showed that Parkin translocated to mitochondria after treatment with STA9090 or NB, comparing to control group (Fig. 4E), and the overall ubiquitination level increased (Fig. 4F). Interestingly, VDAC1 mono-ubiquitination was reduced after Hsp90 C-terminal inhibitor NB treatment, while VDAC1 mono-ubiquitination was not significantly changed after Hsp90 N-terminal inhibitor STA9090 treatment (Fig. 4G). These data suggest that other than the pan-ubiquitination of VDAC1, VDAC1 monoubiquitin modification plays a critical role in VDAC1 oligomerization and mitochondrial-mediated apoptosis pathway. Interestingly, after we transfected VDAC1 K274R mutant plasmid into HepG2 cells, co-immunoprecipitation experiment showed that the interaction between Hsp90α and VDAC1 was significantly weakened (Fig. 4H). Therefore, we conclude that Hsp90α C-terminal inhibition decreases VDAC1 K274 mono-ubiquitination, which promotes VDAC1 oligomerization.

Hsp90 C-terminal inhibitor Novobiocin retards tumor growth and induces tumor apoptosis with increased VDAC1 oligomerization

In vitro, we have proved that Hsp90 C-terminal inhibition promotes VDAC1 oligomerization and initiates mitochondrial apoptosis pathway. To further test this *in vivo*, we injected HepG2-Luc cells as subcutaneous tumor xenografts in nude mice [42]. Tumor luminescence foci in animals treated with Hsp90 C-terminal inhibitor Novobiocin or Hsp90 N-terminal inhibitor STA9090 were smaller than the foci observed in the control (Fig. 5A). Similarly, the average final tumor size was also smaller (Fig. 5B), and the tumors grew slower in the Hsp90 inhibitor treatment group (Fig. 5C). It demonstrated that both two Hsp90 inhibitors inhibited tumor growth, however, the results of chemical cross-linking revealed that only tumors treated with

Hsp90 C-terminal inhibitors formed more VDAC1 oligomers. There was no significant difference in VDAC1oligomerization between the control and Hsp90 N-terminal inhibitor STA9090 treatment groups (Fig. 5D). Consistently, Hsp90 C-terminal inhibitor NB triggered PARP cleavage in tumor cells (Fig. 5E). Identical results were obtained by immunohistochemical analysis (Fig. 5F). These results indicate Hsp90 C-terminal inhibitor Novobiocin significantly promotes VDAC1 oligomerization and induces tumor apoptosis compared with Hsp90 N-terminal inhibitor.

Inhibition of Hsp90 C-terminal domain with Novobiocin increases VDAC1 channel conductance

In this work, Hsp90α and Hsp90 inhibitors (N-terminal inhibitor STA9090 and C-terminal inhibitor Novobiocin) were tested for the effect on Hsp90α-VDAC1 interaction and VDAC1 oligomerization. We reconstituted purified VDAC1 to a planar lipid bilayer and examined its channel characteristics according to the specified protocol (Fig. 6A) [37, 38]. First, we purified VDAC1 from rat liver (Fig. S3A) and reconstituted a planar lipid bilayer (PLB) with purified VDAC1. VDAC1 channel current was successfully recorded (Fig. S3B), and the oligomer inhibitor VBIT-4 significantly inhibited VDAC1 channel conductance (Fig. 6B). After recording the current of the VDAC1 channel in a voltage-clamp at -10mV, Hsp90α was added and incubated for 10min. VDAC1 channel conductance of ~8 nS (-10 mV, in 1 M KCl) was obtained (Fig. 6C). STA9090 or NB was then used and incubated for 10 min. We observed that NB promoted an increase in VDAC1 conductance and the VDAC1 channel conductance was ~10 nS at first (Fig. 6C). Subsequently, the conductance of VDAC1 continues to increase, and it is often observed

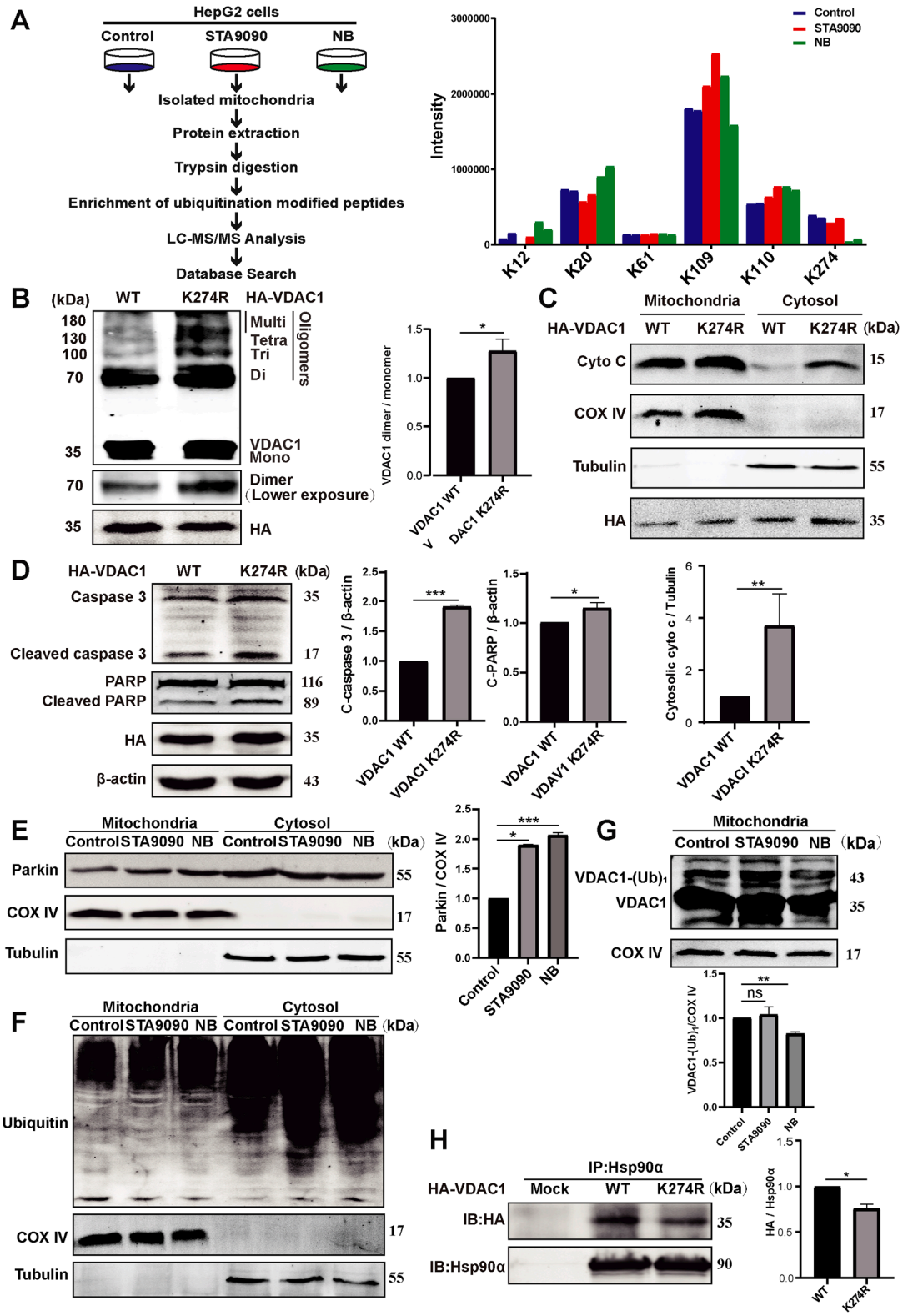

Fig. 4. Hsp90 C-terminal inhibitor Novobiocin inhibits mono-ubiquitination of VDAC1 K274 and promotes oligomerization of VDAC1. **(A)** Mass spectrometric analysis procedure of ubiquitylated mitochondrial proteins (left panel) and different ubiquitylation of VDAC1 K12, K20, K61, K109, K110, and K274 after STA9090 or NB treatment (right panel). The experiment was performed in two biological replicates. **(B)** HepG2 cells were transiently transfected with plasmids encoding HA-tagged VDAC1 WT or K274R for 36 h; Oligomerization of VDAC1 was analyzed by Western blotting after EGS cross-linking. **(C)** The release of cytochrome c was detected by Western blotting. **(D)** The cell lysates were detected by Western blotting for the cleavage of apoptosis-related protein PARP and caspase 3. **(E)** HepG2 cells were incubated w/o STA9090 (100nM) or NB (0.5mM) for 24 h. The level of Parkin translocated to mitochondria was determined by Western blotting. **(F)** Ubiquitination assays for mitochondria and cytosol after STA9090 and NB treatment for 24 h. **(G)** VDAC1 K274R mono-ubiquitination assays after STA9090 and NB treatment for 24 h (Ub1: mono-Ub, Ubn: poly-Ub). **(H)** Co-immunoprecipitation of VDAC1 and Hsp90α was performed with lysates of HepG2 cells after STA9090 or NB treatment. Hsp90α and VDAC1 levels were determined by Western blotting. All data represent mean ± SD, n = 3, *$p < 0.05$, **$p < 0.01$, ***$p < 0.001$.

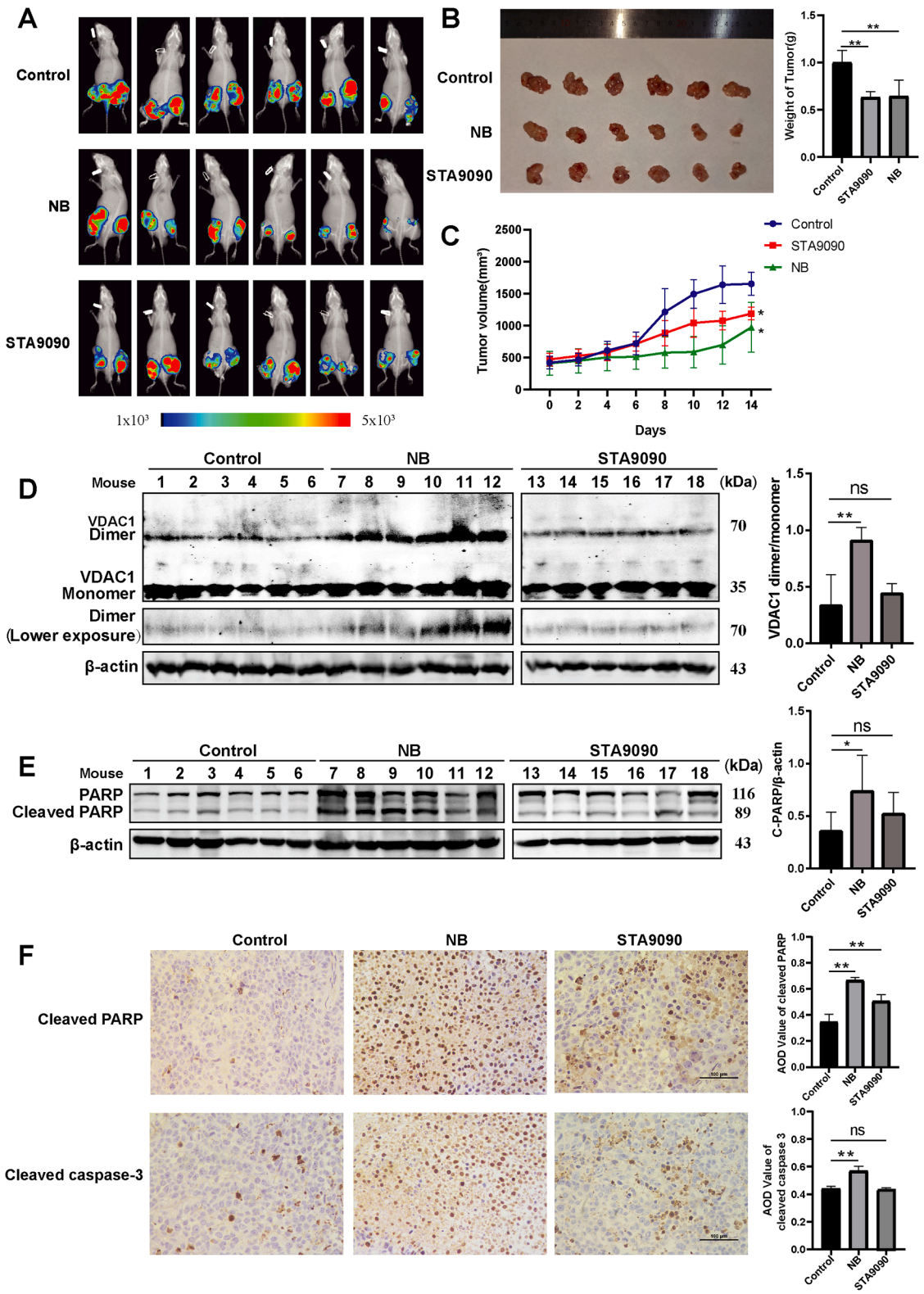

Fig. 5. Hsp90 C-terminal inhibitor Novobiocin promotes VDAC1 oligomerization and apoptosis in tumor xenograft. HepG2-Luc Cells (1×10^7) were injected subcutaneously into nude mice to form xenograft tumors. **(A)** Tumor luminescence foci were visualized using IVIS Lumina XRMS living imaging system 14 days after injection. **(B)** The excised xenograft tumors from control, STA9090-treated and NB-treated mice 14 days after injection of HepG2-Luc cells (left panel) and the tumors' weight (right panel). **(C)** Growth of the xenograft tumor volume every two days was recorded and calculated as $V=0.5 \times L \times W^2$ (V: volume, L: length, W: width). (D) VDAC1 oligomerization of xenograft tumors were visualized by Western blot analysis after treatment with cross-linking reagent EGS (500 μM). Each lane represents different mouse. (E) The level of cleavage-PARP from xenograft tumors was determined by Western blot analysis. Each lane represents different mouse. **(F)** Immunohistochemistry staining with cleaved-PARP and cleaved-caspase 3 antibodies on dissection samples from xenografted tumors. Scale bar is 100 μm. Quantification of the immunohistochemistry images were analyzed by ImageJ software v1.8.0 (NIH, MD, USA) as average optical density (AOD) [AOD = Integrated Optical Density (IOD) SUM/Area SUM]. Quantitative data are mean ± SD of n = 6 mice per group. *$p < 0.05$, **$p < 0.01$.

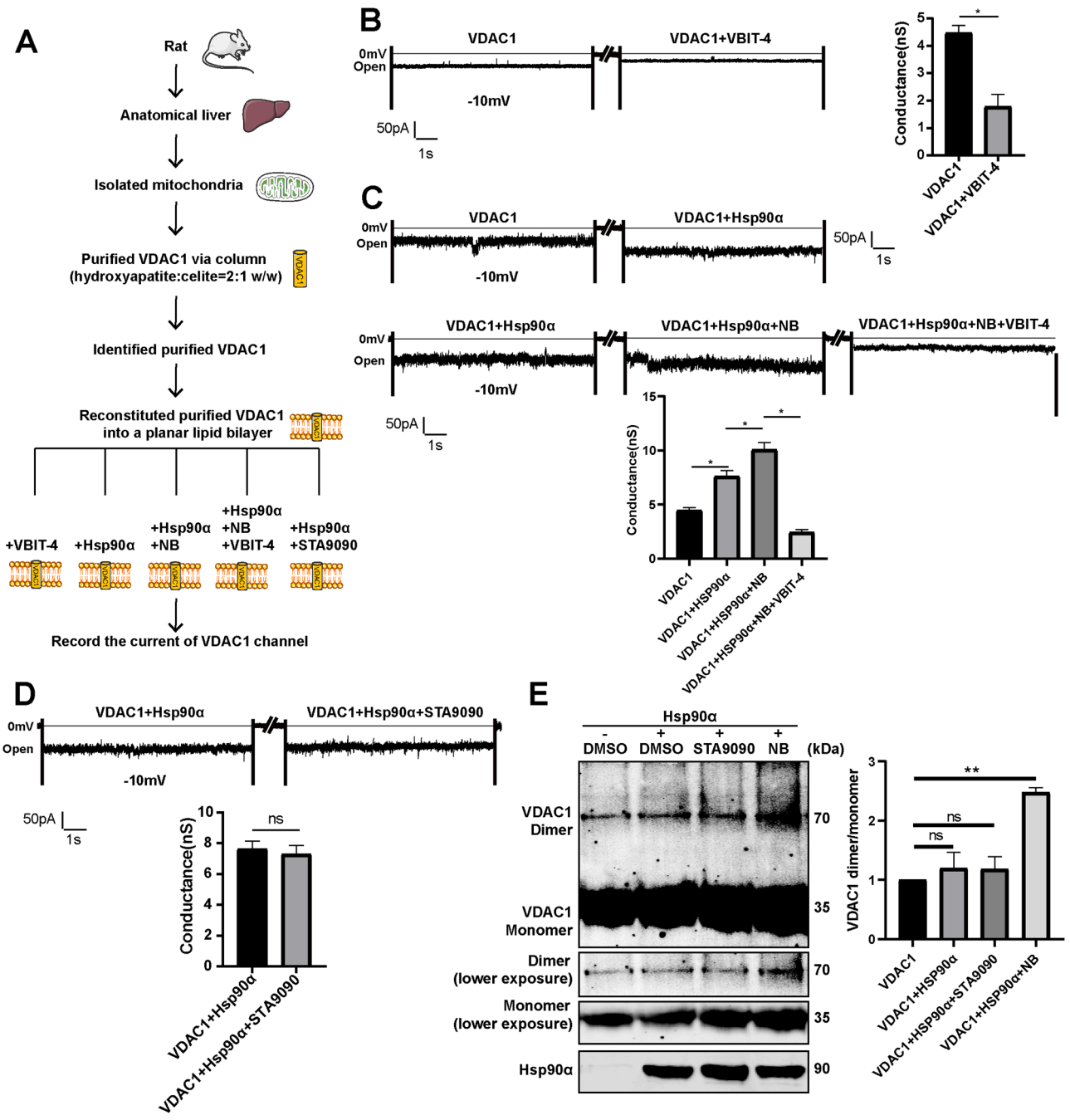

Fig. 6. VDAC1-specific oligomerization inhibitor VBIT-4 reduces Hsp90 C-terminal inhibitor Novobiocin – increased VDAC1 channel conductance. **(A)** The protocol of patch clamp experiment by reconstituting VDAC1 purified from rat liver mitochondria to planar lipid bilayer. **(B)** VDAC1 was reconstituted into a PLB and currents through VDAC1, in response to a voltage step from 0 to -10 mV, were recorded before and 30 min after the addition of VBIT-4 (40 μM) **(C)** VDAC1 was reconstituted into a PLB and currents through VDAC1, in response to a voltage step from 0 to -10 mV, were recorded before and after the addition of Hsp90α (Top panel). Purified VDAC 1 and Hsp90α protein were added to the cis side of the PLB and channel conductance was recorded following Novobiocin (NB) or NB combined with VBIT-4 treatment (Bottom panel). **(D)** Purified VDAC1 protein and Hsp90α protein treated with STA9090 were added to the cis side of the PLB and channel conductance was recorded. Quantitative data are mean ± SD, n=6. $*p < 0.05$. **(E)** Purified VDAC1 protein(5 μg) was incubated with Hsp90α protein or STA9090 or NB-treated Hsp90α protein for 10min (VDAC1: Hsp90α=3:1). VDAC1 oligomerization of purified VDAC1 protein was visualized by Western blot analysis after treatment with cross-linking reagent EGS (500 μM). All data represent mean ± SD, n = 3, $**p < 0.01$.

that the high conductance of VDAC1 causes the breakdown of the PLB after NB addition (Fig. S3C). However, the change of VDAC1 channel conductance was not obviously changed after adding STA9090 (Fig. 6D). In addition, VBIT-4 successfully reduced the conductance of VDAC1 after NB addition and VDAC showed stable, long-lived conducting states of ~2.5 nS, as recorded in several separate experiments, performed under the same conditions (-10 mV, 1 M KCl) (Fig. 6B). Based on the current traces of VDAC1 after NB treatment, VDAC1 in the PLB is likely to form oligomers. To test this hypothesis, we used purified VDAC1 and its incubation in the absence and the presences Hsp90α or Hsp90α treated with STA9090 or NB and performed cross-linking to demonstrate the direct effect of Hsp90α on VDAC1 oligomerization (Fig. S3D). The results showed that there was no significant change in VDAC1 oligomers after incubation of purified VDAC1 with Hsp90α

protein. However, only NB-treated Hsp90α protein promoted VDAC1 oligomerization, but not STA9090 treatment (Fig. 6E). In addition, when VDAC1 was incubated with STA9090 or NB alone, no significant changes in VDAC1 oligomers were observed (Fig. S3E). Taken together, these results can support the interaction of Hsp90 with VDAC1 directly and inhibition of Hsp90 C-terminal domain increases VDAC1 channel conductance and promotes VDAC1 oligomerization.

Discussion

Accumulated evidence suggests Hsp90 C-terminal inhibitor using the new inhibitory scaffold further enhances the ability to inhibit cancer cell proliferation, promote apoptosis and inhibit tumor growth [43]. These approaches have led to alleviation of adverse off-target effects caused by pan-inhibition of Hsp90 using N-terminal inhibitors [17]. Despite progress made thus far, the mechanism for Hsp90 C-terminal inhibitors remains mysterious and the role of Hsp90 C-terminal inhibitors in hepatocellular carcinoma has rarely been studied. Because of adverse reactions and drug resistance of Hsp90 N-terminal inhibitors in the treatment process, the study of the mechanism of Hsp90 C-terminal inhibitors may provide a new therapeutic strategy for HCC.

In this study, we demonstrate that Hsp90 C-terminal inhibitor Novobiocin decreases VDAC1 K274 mono-ubiquitination which promotes VDAC1 oligomerization, channel conductance, cytochrome c release from mitochondria and apoptosis (Fig. 7).

VDAC1 pore size at high conductance state is about 2.6-3nm, sufficient to pass through nucleotides and small molecules up to 5 kDa, but not a folded protein like Cyto c (12 kDa). Interestingly, VDAC1 oligomerization forms a large channel to export pro-apoptotic proteins in IMS to the cytoplasm to initiate apoptosis [6,44]. No matter what type of cells are studied, apoptosis inducers such as H_2O_2, curcumin, STS, As_2O_3, cisplatin, selenite, epposide, TNF-α and UV light can induce VDAC1 oligomerization to release Cyto c and thus initiate apoptosis [10, 11,45]. In this study, our results show that Hsp90 C-terminal inhibitor NB significantly promotes VDAC1 oligomerization, cytochrome c release and initiates mitochondrial apoptosis pathway, comparing to the effect of Hsp90 N-terminal inhibitor STA9090. In addition, the conductance properties of VDAC1 were examined following reconstitution into a planar lipid bilayer. Our results demonstrate that Hsp90 C-terminal domain inhibition increases the conductance of VDAC1 channel while inhibiting the N-terminal domain of Hsp90 does not significantly change the conductance of VDAC1 channel. Although VBIT-4, a specific VDAC1 oligomer inhibitor, was used to successfully inhibit the NB-induced increase in VDAC1 channel conductance, it has not been proved that VBIT-4 inhibits VDAC1 channel conductance through VDAC1 oligomerization. Therefore, the relationship between VBIT-4 inhibition of VDAC1 channel conductance and VDAC1 oligomerization needs to be further verified. However, our results showed that NB significantly promoted purified VDAC1 oligomerization after co-incubation of purified VDAC1 with Hsp90α protein. It is possible to explain that the NB-induced increase in VDAC1 channel conductance is related to the promotion of VDAC1 oligomerization. In addition, Smilansky [46] et al. showed that the interaction between amyloid beta and VDAC1 increased VDAC1 channel conductance, which may be due to the insertion of amyloid beta into the VDAC1 β-barrel [47] or induction of VDAC1 oligomerization by amyloid beta oligomers. This also provides a possibility to explain that Hsp90α and NB increase VDAC1 channel conductance. Anyway, further studies are required to explore the detailed mechanism by which Hsp90α and NB increases VDAC1 channel conductance.

In this study, our results show that Hsp90 C-terminal inhibitor NB reduces VDAC1 K274 mono-ubiquitination to promote VDAC1 oligomerization and initiate mitochondrial apoptosis pathway. The three-dimensional structure of VDAC1 at atomic resolution [48,49] shows that VDAC1 adopts a β-barrel structure consisting of 19 β-strands with the horizontally oriented α-helix N-terminal located in the middle of the pore. The N-terminal domain of VDAC1 exists in a dynamic equilibrium, located within the pore or exposed to the cytoplasm. Mobility of VDAC1 N-terminal region is important for VDAC1 dimerization, channel gating and proteins associated with apoptosis [50,51]. Our results show that Hsp90 interacts with VDAC1 monomers or dimers on the cytoplasmic side in atomic coarse particle simulation and inhibition of HSP90 C-terminal domain promotes VDAC1 oligomerization. This suggests that Hsp90 may interact with VDAC1 through the N-terminal region of VDAC1. In addition, using site-directed mutation, a combination of cysteine substitution, chemical cross-linkers, and computational analysis to identify contact sites in VDAC1 oligomers under physiological and apoptotic conditions, the study identified two forms of dimeric

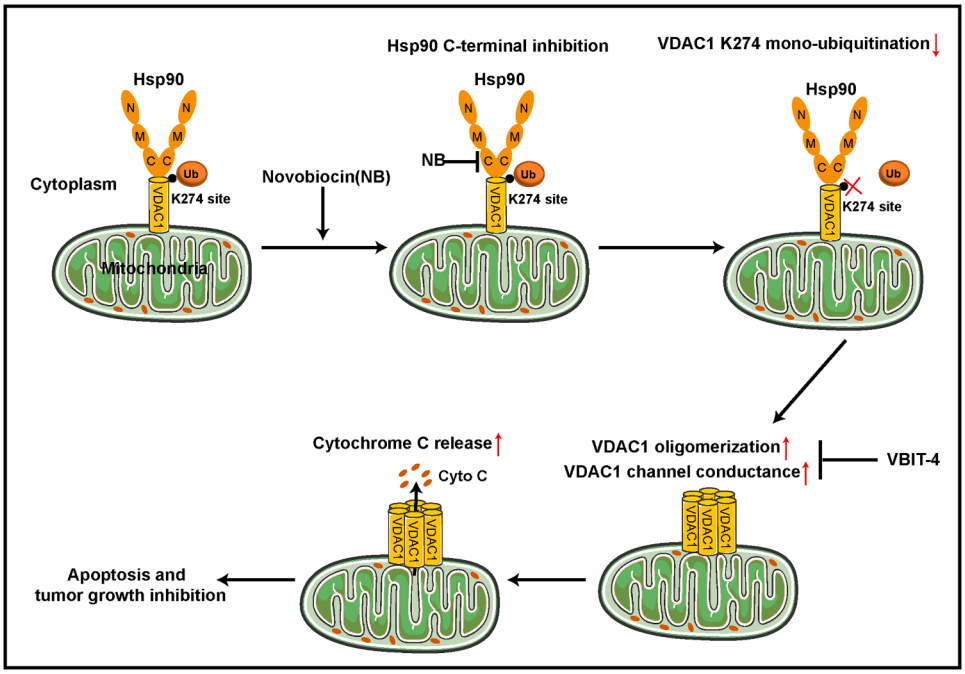

Fig. 7. Hsp90 C-terminal inhibitor Novobiocin decreases VDAC1 K274 mono-ubiquitination which promotes VDAC1 oligomerization, channel conductance, cytochrome c release and apoptosis. Hsp90 C-terminal inhibitor NB weakens the stability of VDAC1 monomer by disrupting VDAC1 K274 mono-ubiquitination and promotes VDAC1 oligomerization. Thus, the release of cytochrome c from the mitochondrial membrane gap initiates mitochondrial apoptosis pathway. The VDAC1-specific oligomerization inhibitor VBIT-4 alleviates Novobiocin-induced VDAC1 oligomerization, cytochrome c release and apoptosis.

VDAC1, one contact site involving beta strands 1, 2 and 19, and a second one involving beta strands 16 and 17 [52]. The β strands 1 and 19 are arranged in parallel, where the N-terminal region of VDAC1 lies inside the pore and can flick out of it [6]. This further supports that the N-terminal region of VDAC1 may play an important role in the oligomerization of VDAC1. Consistently, VDAC1 K274 is located at β strand 19, which might explain why VDAC1 K274 mutation promotes VDAC1 oligomerization. Previous studies demonstrated that reducing VDAC1 K274 mono-ubiquitination could induce apoptosis but did not explain the effect of VDAC1 K274 mono-ubiquitination on VDAC1 oligomerization [29]. In this study, we demonstrated that inhibition of Hsp90 C-terminal reduces VDAC1 K274 mono-ubiquitination and promotes VDAC1 oligomerization. Interestingly, the mutation of VDAC1 (K274R) weakens the interaction between Hsp90 and VDAC1. This means that VDAC1 K274 mono-ubiquitination plays an important role in the interaction between VDAC1 and Hsp90 and maintains the stability of VDAC1 monomer.

In vivo experiments, we also confirm that NB can significantly promote VDAC1 oligomers comparing to STA9090. Interestingly, both Hsp90 inhibitors had the same inhibitory effect on tumor growth despite their inconsistent apoptosis-induced effects. According to our proteomic results, the differentially expressed proteins in the STA9090 treatment group were mainly enriched in cell division and mitotic nuclear division. These results indicate that STA9090 mainly acts on cell proliferation in HCC. However, this study confirms that STA9090 doesn't inhibit tumor cell growth by VDAC1 oligomerization-related apoptosis. Hsp90 is involved in a variety of cell signaling pathways and stress responses, and plays a critical role in cell survival. In dysfunctional tissues, HSP90-mediated regulatory mechanisms are involved in various types of programmed cell death, including apoptosis, autophagy, necroptosis, ferroptosis, and others [53]. Studies have shown that STA9090 analogues GA, 17-AAG and 17-DMAG can induce non-apoptotic programmed cell death, such as necroptosis and autophagy, in addition to inducing classical apoptosis [54–56]. Hence, although STA9090 inhibitor did not significantly initiate the mitochondrial apoptosis pathway, they might inhibit tumor growth through other cell death pathway in HCC. In addition, although STA9090 also induced tumor growth inhibition, our previous research results showed that STA9090 induced VPS35-related extracellular vesicles release and metastasis, thus inducing the unexpected metastasis via extracellular vesicles induction in hepatocellular carcinoma, which was seldomly observed in NB treated nude mice [42]. Similar results have also been reported, such as Hsp90 inhibitor 17-DMAG effectively inhibited liver metastasis in chemotherapy-refractory small cell lung cancer (SCLC), but aggravated bone metastasis [25]. In addition, Hsp90 inhibitor 17-AAG significantly reduced the growth of MDA-MB-231SA tumors in breast fat pad of nude mice, but increased the incidence of bone metastasis and osteolytic lesions in nude mice [26]. These findings suggest that the N-terminal Hsp90 inhibitor has a potential role in promoting tumor metastasis, but it is rarely observed in the C-terminal Hsp90 inhibitor NB. In contrast, our results show that NB significantly inhibits cell metastasis through VDAC1 oligomerization related apoptosis, and inhibiting VDAC1 oligomerization instead promotes cell metastasis. Hence, other than tumor growth inhibition, NB-induced metastasis inhibition, that is the clinical significance, better than Hsp90 N-terminal inhibitor STA9090.

Conclusion

Hsp90 C-terminal inhibition promotes VDAC1-oligomerization-related apoptosis by decreasing VDAC1 K274 mono-ubiquitination. Targeting mitochondrial protein VDAC1 via Hsp90 C-terminal inhibitor and the elucidation of the mechanism beneath will provide a new perspective for mitochondria-targeted therapy of HCC.

Ethics statement

The animal research ethics committee of Southern Medical University approved all the animal experimental procedures;

CRediT authorship contribution statement

Jinxin Zhang: Conceptualization, Data curation, Formal analysis, Investigation, Methodology, Writing – original draft. **Lixia Liu:** Methodology, Writing – review & editing. **Yan Li:** Data curation, Methodology. **Yaling Huang:** Data curation, Methodology. **Senbo Xiao:** Data curation, Formal analysis, Investigation, Methodology. **Zihao Deng:** Data curation. **Zhenming Zheng:** Data curation. **Jieyou Li:** Data curation. **Manfeng Liang:** Data curation. **Guantai Xie:** Data curation. **Xiao Chen:** Data curation. **Yaotang Deng:** Data curation. **Wenchong Tan:** Data curation. **Hairou Su:** Data curation. **Guibing Wu:** Data curation. **Chunqing Cai:** Data curation. **Xuemei Chen:** Conceptualization, Funding acquisition, Project administration, Resources, Supervision, Writing – original draft. **Fei Zou:** Conceptualization, Funding acquisition, Project administration.

Declaration of Competing Interest

The authors declare no conflict of interest and all authors have given their consent for the manuscript to be published

Data availability

Data are available upon request from the corresponding author.

Funding

This work was supported by grants from the National Natural Science Foundation of China No. 82072105 and 81673216 to Xuemei Chen (NSFC) and No.82130054 and 81971783 to Fei Zou

Acknowledgments

We thank Nanomechanical Lab (Nanomechanical Lab - NTNU) Department of Structural Engineering Norwegian University of Science and Technology Trondheim, Norway for Coarse-grained molecular systems containing Hsp90, VDAC1.

Reference

[1] K Hajiasgharzadeh, MH Somi, D Shanehbandi, A Mokhtarzadeh, B Baradaran, Small interfering RNA-mediated gene suppression as a therapeutic intervention in hepatocellular carcinoma, J. Cell Physiol. 234 (4) (2019) 3263–3276.
[2] S Chen, Q Cao, W Wen, H Wang, Targeted therapy for hepatocellular carcinoma: challenges and opportunities, Cancer Lett 460 (2019) 1–9.
[3] Q Chen, D Jia, J Ren, Y Cheng, H Wu, S Guo, et al., VDAC1 balances mitophagy and apoptosis in leafhopper upon arbovirus infection, Autophagy 2022 (2022) 1–15.
[4] U Anand, A Shteinfer-Kuzmine, G Sela, M Santhanam, B Gottschalk, R Boujemaa-Paterski, et al., The multicellular effects of VDAC1 N-terminal-derived peptide, Biomolecules 12 (10) (2022) 1387.
[5] NN Wu, Y Bi, A Ajoolabady, F You, J Sowers, Q Wang, et al., Parkin insufficiency accentuates high-fatdiet-induced cardiac remodeling and contractile dysfunction through VDAC1-mediated mitochondrial Ca^{2+} overload, JACC Basic Transl. Sci. 7 (8) (2022) 779–796.
[6] V Shoshan-Barmatz, A Shteinfer-Kuzmine, A Verma, VDAC1 at the intersection of cell metabolism, apoptosis, and diseases, Biomolecules 10 (11) (2020) 1485.
[7] V Shoshan-Barmatz, S Pittala, D Mizrachi, VDAC1 and the TSPO: expression, interactions, and associated functions in health and disease states, Int. J. Mol. Sci. 20 (13) (2019) 3348.
[8] A Shteinfer-Kuzmine, S Argueti-Ostrovsky, MF Leyton-Jaimes, U Anand, S Abu-Hamad, R Zalk, et al., Targeting the mitochondrial protein VDAC1 as a potential therapeutic strategy in ALS, Int. J. Mol. Sci. 23 (17) (2022) 9946.
[9] Y He, W Wang, T Yang, ER Thomas, R Dai, X Li, The potential role of voltage-dependent anion channel in the treatment of Parkinson's disease, Oxid. Med. Cell Longev. 2022 (2022), 4665530.

[10] KA Heslop, P Burger, C Kappler, AK Solanki, M Gooz, YK Peterson, et al., Small molecules targeting the NADH-binding pocket of VDAC modulate mitochondrial metabolism in hepatocarcinoma cells, Biomed. Pharmacother. 150 (2022), 112928.
[11] S Liu, JJ Aweya, L Zheng, Z Zheng, H Huang, F Wang, et al., LvHemB1, a novel cationic antimicrobial peptide derived from the hemocyanin of Litopenaeus vannamei, induces cancer cell death by targeting mitochondrial voltage-dependent anion channel 1, Cell Biol. Toxicol. 38 (1) (2022) 87–110.
[12] A Verma, A Shteinfer-Kuzmine, N Kamenetsky, S Pittala, A Paul, E Nahon Crystal, et al., Targeting the overexpressed mitochondrial protein VDAC1 in a mouse model of Alzheimer's disease protects against mitochondrial dysfunction and mitigates brain pathology, Transl. Neurodegener. 11 (1) (2022) 58.
[13] V Shoshan-Barmatz, D Ben-Hail, L Admoni, Y Krelin, SS Tripathi The mitochondrial voltage-dependent anion channel 1 in tumor cells, Biochim. Biophys. Acta. 1848 (10) (2015) 2547–2575.
[14] J Zhang, H Li, Y Liu, K Zhao, S Wei, ET Sugarman, et al., Targeting hsp90 as a novel therapy for cancer: mechanistic insights and translational relevance, Cells 11 (18) (2022) 2778.
[15] MP Sumi, A Ghosh, Hsp90 in human diseases: molecular mechanisms to therapeutic approaches, Cells 11 (6) (2022) 976.
[16] BJ Lang, TL Prince, Y Okusha, H Bunch, SK Calderwood, Heat shock proteins in cell signaling and cancer, Biochim. Biophys. Acta. Mol. Cell Res. 1869 (3) (2022), 119187.
[17] E Amatya, BSJ Blagg, Recent advances toward the development of hsp90 C-terminal inhibitors, Bioorg. Med. Chem. Lett. 80 (2023), 129111, 2023.
[18] Z Li, Y Luo, Hsp90 inhibitors and cancer: prospects for use in targeted therapies (review), Oncol. Rep. 49 (1) (2023) 6.
[19] Z Yuan, L Wang, C Chen, Analysis of the prognostic, diagnostic and immunological role of hsp90α in malignant tumors, Front. Oncol. 12 (2022), 963719.
[20] PA Konstantinopoulos, S Cheng, JG Supko, M Polak, AE Wahner-Hendrickson, SP Ivy, et al., Combined PARP and hsp90 inhibition: preclinical and phase I evaluation in patients with advanced solid tumours, Br. J. Cancer. 126 (7) (2022) 1027–1036.
[21] S Slovin, S Hussain, F Saad, J Garcia, J Picus, R Ferraldeschi, et al., Pharmacodynamic and clinical results from a phase I/II study of the hsp90 inhibitor onalespib in combination with abiraterone acetate in prostate cancer, Clin. Cancer Res. 25 (15) (2019) 4624–4633.
[22] C Wang, Y Zhang, K Guo, N Wang, H Jin, Y Liu, W Qin, Heat shock proteins in hepatocellular carcinoma: molecular mechanism and therapeutic potential, Int. J. Cancer. 138 (8) (2016) 1824–1834.
[23] M Nouri-Vaskeh, L Alizadeh, K Hajiasgharzadeh, A Mokhtarzadeh, M Halimi, B Baradaran, The role of hsp90 molecular chaperones in hepatocellular carcinoma, J. Cell Physiol 235 (12) (2016) 9110–9120.
[24] X Ren, T Li, W Zhang, X Yang, Targeting heat-shock protein 90 in cancer: an update on combination therapy, Cells 11 (16) (2022) 2556.
[25] S Takeuchi, K Fukuda, S Arai, S Nanjo, K Kita, T Yamada, et al., Organ-specific efficacy of hsp90 inhibitor in multiple-organ metastasis model of chemorefractory small cell lung cancer, Int. J. Cancer. 138 (5) (2016) 1281–1289.
[26] JT Price, JMW Quinn, NA Sims, J Vieusseux, K Waldeck, SE Docherty, et al., The heat shock protein 90 inhibitor, 17-allylamino-17-demethoxygeldanamycin, enhances osteoclast formation and potentiates bone metastasis of a human breast cancer cell line, Cancer Res. 65 (11) (2005) 4929–4938.
[27] M Marcu, T Schulte, L Neckers, Novobiocin and related coumarins and depletion of heat shock protein 90-dependent signaling proteins, J. Natl. Cancer Inst 92 (3) (2000) 242–248.
[28] MG Marcu, A Chadli, I Bouhouche, M Catelli, LM Neckers, et al., The heat shock protein 90 antagonist novobiocin interacts with a previously unrecognized ATP-binding domain in the carboxyl terminus of the chaperone, J. Biol. Chem. 275 (47) (2000) 37181–371816.
[29] SJ Ham, D Lee, H Yoo, K Jun, H Shin, J Chung, et al., Decision between mitophagy and apoptosis by parkin via VDAC1 ubiquitination, Proc. Natl. Acad. Sci. U S A. 117 (8) (2020) 4281–4291.
[30] X Zhou, Y Wen, Y Tian, M He, X Ke, Z Huang, et al., Heat shock protein 90α-dependent b-cell-2-associated transcription factor 1 promotes hepatocellular carcinoma proliferation by regulating MYC proto-oncogene c-MYC mRNA stability, Hepatol. 69 (4) (2019) 1564–1581.
[31] M Morgenstern, CD Peikert, P Lübbert, I Suppanz, C Klemm, O Alka, et al., Quantitative high-confidence human mitochondrial proteome and its dynamics in cellular context, Cell Metab 33 (12) (2021) 2464–2483.
[32] J Kim, R Gupta, LP Blanco, S Yang, A Shteinfer-Kuzmine, K Wang, et al., VDAC oligomers form mitochondrial pores to release mtDNA fragments and promote lupus-like disease, Science 6472 (366) (2019) 1531–1536.
[33] HR Bridges, JG Fedor, JN Blaza, A Di Luca, A Jussupow, OD Jarman, et al., Structure of inhibitor-bound mammalian complex I, Nat. Commun. 11 (1) (2020) 5261.
[34] MMU Ali, SM Roe, CK Vaughan, P Meyer, B Panaretou, PW Piper, et al., Crystal structure of an hsp90-nucleotide-p23/sba1 closed chaperone complex, Nature 440 (7087) (2006) 1013–1017.
[35] M Bayrhuber, T Meins, M Habeck, S Becker, K Giller, S Villinger, et al., Structure of the human voltage-dependent anion channel, Proc. Natl. Acad. Sci. U S a. 105 (40) (2008) 15370–15375.
[36] TA Wassenaar, HI Ingólfsson, RA Böckmann, DP Tieleman, SJ Marrink, Computational lipidomics with insane: a versatile tool for generating custom membranes for molecular simulations, J. Chem. Theory. Comput. 11 (5) (2015) 2144–2155.
[37] D Ben-Hail, V. Shoshan-Barmatz, Purification of vdac1 from rat liver mitochondria, Cold Spring Harb. Protoc. 2014 (1) (2014) 94–99.
[38] D Ben-Hail, V. Shoshan-Barmatz, Reconstitution of purified vdac1 into a lipid bilayer and recording of channel conductance, Cold Spring Harb. Protoc. 2014 (1) (2014) 100–105.
[39] D Ben-Hail, R Begas-Shvartz, M Shalev, A Gruzman, V Shoshan-Barmatz Novel compounds targeting the mitochondrial protein VDAC1 inhibit apoptosis and protects against mitochondrial dysfunction, J. Biol. Chem. 291 (48) (2016) 24986–25003.
[40] MF Tomasello, F Guarino, S Reina, A Messina, V De Pinto, The voltage-dependent anion selective channel 1 (VDAC1) topography in the mitochondrial outer membrane as detected in intact cell, PLoS. One. 8 (12) (2013) e81522.
[41] Y Liao, Y Hao, H Chen, Q He, Z Yuan, J Cheng mitochondrial calcium uniporter protein MCU is involved in oxidative stress-induced cell death, Protein. Cell. 6 (6) (2015) 434–442.
[42] W Tan, J Zhang, L Liu, M Liang, J Li, Z Deng, et al., Hsp90 inhibitor sta9090 induced vps35 related extracellular vesicle release and metastasis in hepatocellular carcinoma, Transl. Oncol. 26 (2022), 101502.
[43] MK Kurop, CM Huyen, JH Kelly, BSJ Blagg, The heat shock response and small molecule regulators, Eur. J. Med. Chem. 226 (2021), 113846.
[44] N Keinan, D Toymkin, V Shoshan-Barmatz, Oligomerization of the mitochondrial protein VDAC is coupled to the induction of apoptosis, Mol. Cell Biol 30 (24) (2010) 5698–5709.
[45] Z Zalk, A Israelson, E Garty, H Azoulay- Zohar, V Shoshan-Barmatz, Oligomeric states of the voltage-dependent anion channel and cytochrome c release from mitochondria, Biochemical. J 386 (2005) 73–83.
[46] A Smilansky, L Dangoor, I Nakdimon, D Ben-Hail, D Mizrachi, V Shoshan-Barmatz, The voltage-dependent anion channel 1 mediates amyloid β toxicity and represents a potential target for alzheimer disease therapy, J. Biol. Chem. 290 (52) (2015) 30670–30683.
[47] F.P Thinnes, New findings concerning vertebrate porin II: on the relevance of glycine motifs of type-1 VDAC, Mol. Genet. Metab. 108 (2013) 212–224.
[48] J Preto, H Gorny, I Krimm, A deep dive into VDAC1 conformational diversity using all-atom simulations provides new insights into the structural origin of the closed states, Int. J. Mol. Sci. 23 (3) (2022) 1175.
[49] EE Najbauer, K Tekwani Movellan, K Giller, R Benz, S Becker, C Griesinger, LB Andreas, Structure and gating behavior of the human integral membrane protein VDAC1 in a lipid bilayer, J. Am. Chem. Soc. 144 (7) (2022) 2953–2967.
[50] S Geula, D Ben-Hail, V Shoshan-Barmatz, Structure-based analysis of VDAC1: N-terminus location, translocation, channel gating and association with anti-apoptotic proteins, Biochem. J. 444 (3) (2012) 475–485.
[51] V Shoshan-Barmatz, Y Krelin, Q Chen, VDAC1 as a player in mitochondria-mediated apoptosis and target for modulating apoptosis, Curr. Med. Chem. 24 (40) (2017) 4435–4446.
[52] S Geula, H Naveed, J Liang, V Shoshan-Barmatz, Structure-based analysis of VDAC1 protein: defining oligomer contact sites, J. Biol. Chem. 287 (3) (2012) 2179–2190.
[53] C Peng, F Zhao, H Li, L Li, Y Yang, F Liu, Hsp90 mediates the connection of multiple programmed cell death in diseases, Cell Death Dis 13 (11) (2022) 929.
[54] W Chen, H Yu, H Fan, C Zhang, M Zhang, C Zhang, et al., Rip1 mediates the protection of geldanamycin on neuronal injury induced by oxygen-glucose deprivation combined with zvad in primary cortical neurons, J. Neurochem. 120 (1) (2012) 70–77.
[55] X Yu, M Mao, X Liu, T Shen, et al., A cytosolic heat shock protein 90 and co-chaperone p23 complex activates ripk3/mlkl during necroptosis of endothelial cells in acute respiratory distress syndrome, J. Mol. Med. 98 (4) (2020) 569–583.
[56] X Yu, M Mao, X Liu, T Shen, T Li, H Yu, et al., 17-DMAG disrupted the autophagy flux leading to the apoptosis of acute lymphoblastic leukemia cells by inducing heat shock cognate protein 70, Life Sci 249 (2020), 117532.